

Launching Light into a Fiber

MASUD MANSURIPUR

A typical single-mode silica glass fiber has a mode profile that is well approximated by a Gaussian beam. At $\lambda = 1.55 \mu\text{m}$, this Gaussian mode has a ($1/e^2$ intensity) diameter of $\sim 10 \mu\text{m}$. One method of launching light into a fiber calls for placing the polished end of the fiber in contact with (or in close proximity to) the polished end of another (signal-carrying) fiber that has a matching mode profile. Alternatively, a coherent beam of light may be focused directly onto the polished end of the fiber. If the focused spot is well aligned with the fiber's core and has the same amplitude and phase distribution as the fiber's mode profile, then the launched mode will carry the entire incident optical power into the fiber. In general, however, the focused spot is neither perfectly matched to the fiber's mode, nor is it completely aligned with the core. Under these circumstances, only a certain fraction of the incident optical power will be launched into the fiber. The numerical value of this fraction, commonly referred to as the coupling efficiency, will be denoted by η throughout this article.

It is well-known that the strength of the launched mode may be computed by evaluating the overlap integral between the mode profile and the (complex) light amplitude distribution that arrives at the polished facet of the fiber.¹⁻³ The problem of computing the coupling efficiency η is thus reduced to determining the light amplitude distribution immediately in front of the fiber. In what follows, we will evaluate the performance and tolerances of three different lenses designed for coupling a collimated beam of light into a single-mode fiber.

Radial GRIN lens

The first lens to be studied is a radial gradient-index (GRIN) lens, shown schematically in Fig. 1. This lens has plane surfaces on its front and rear sides, which may be antireflection

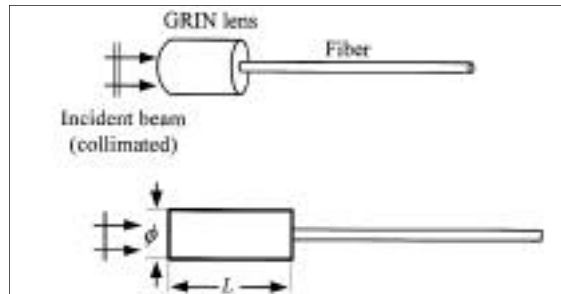


Figure 1. Radial gradient-index (GRIN) lens designed to focus a collimated beam of light into a single-mode fiber attached to its rear facet. In our simulations the lens diameter $\phi = 3.0 \text{ mm}$, length $L = 7.89 \text{ mm}$. The single-mode silica glass fiber has a Gaussian mode profile whose diameter at the $1/e^2$ intensity point is $10 \mu\text{m}$.

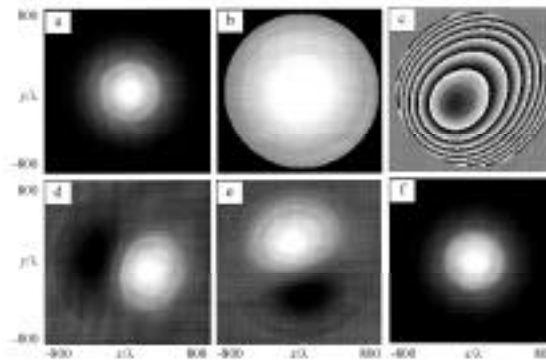


Figure 2. Cross-sectional plots of (a) intensity, (b) log_intensity, (c) phase of a $\lambda = 1.55 \mu\text{m}$ beam arriving at the entrance facet of the GRIN lens of Fig. 1. The intensity distribution is Gaussian, having $D_{\text{FWHM}} = 589\lambda = 0.912 \text{ mm}$, and full-aperture diameter $D = 1500\lambda = 2.325 \text{ mm}$. The Poynting vector distribution $S(x, y)$ —representing geometric-optical rays—is readily computed from the beam profile. Frames (d)-(f) show the x -, y -, z -components of the Poynting vector, namely, $S_x(x, y)$, $S_y(x, y)$, $S_z(x, y)$. In (d) the values of S_x range from -0.18 to $+0.39$. Similarly, S_y in (e) ranges from -0.22 to $+0.32$, and S_z in (f) ranges from 0 to 100 (black = minimum, white = maximum).

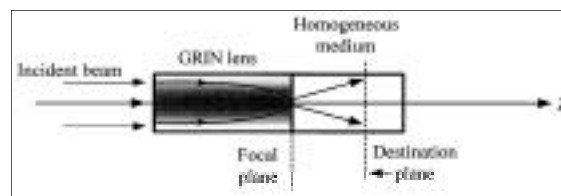


Figure 3. Method of computing the light-amplitude-distribution at the focal plane of the GRIN lens. Ray-tracing begins at the entrance facet, and continues through the focal plane to the destination plane, which is in the far field of the focused spot. At the destination plane the traced rays are used to construct the emergent wavefront, which is subsequently back-propagated (using the far-field or Fraunhofer formula of the classical diffraction theory) to the focal plane at the exit facet of the GRIN lens.

coated to reduce ordinary reflection losses at both facets. The lens diameter $\phi = 3.0 \text{ mm}$, its length $L = 7.89 \text{ mm}$, and its refractive index profile $n(r) = n_0[1 - q(r/r_{\text{max}})^2]$, where $n_0 = 1.5901$, $q = 0.04455$, $r_{\text{max}} = 1.5 \text{ mm}$. The lens is permanently affixed to a single-mode fiber whose guided mode diameter (at the $1/e^2$ intensity point) is $10 \mu\text{m}$.

A collimated Gaussian beam, having radius r_0 (at the $1/e^2$ intensity point) and some wavefront aberration, is incident on the front facet of the lens. Figure 2, top row, shows cross-sectional plots of intensity, log_intensity, and phase for this $\lambda = 1.55 \mu\text{m}$ beam arriving at the entrance facet of the GRIN lens. The intensity profile has $r_0 = 500\lambda$, full-width-at-half-maximum-in-intensity diameter $D_{\text{FWHM}} = 2 \ln 2 r_0 = 0.912 \text{ mm}$, and full-aperture diameter $D = 2.325 \text{ mm}$. The Poynting vector distribution (representing geometric-optical rays) in the cross-sectional plane of the beam is computed, and its x -, y -, z -components are shown in Figs. 2 (d) - (f).

Method of computation

With reference to Fig. 3, we describe a method of computing the (complex) light amplitude distribution at the focal plane of the lens. From the incident beam profile we derive a large number of rays (i.e., Poynting vectors) for subsequent tracing through the system. Ray-tracing begins at the entrance facet of the GRIN lens, and continues through the focal plane to the destination plane, which is in the far field of the focused spot. Note that, after traversing the GRIN lens, the rays emerge into a homogeneous medium of refractive index $n = 1.5$; this region is intended to simulate the medium of the fiber (ignoring the slight difference between the core and cladding indices). At the destination plane the traced rays are used to construct the wavefront of

the emerging (divergent) beam. This wavefront is then propagated backwards, to the focal plane of the GRIN lens (which is located at its exit facet), where the focused spot's diffraction pattern is computed. The reason for tracing the rays all the way to the destination plane (in the far field of the focused spot), constructing the wavefront, then back-propagating to the focal plane is that geometric-optical ray-tracing does not yield valid results when the rays terminate in focal (or caustic) regions.

Figure 4 shows the results of two different computations for the incident beam depicted in Fig. 2. Shown are the intensity and phase distributions at the focal plane of the GRIN lens of Fig. 3. The incident wavefront is initially converted to a set of geometric-optical rays, using the association between a ray and the local Poynting vector of the electromagnetic field. In Figs. 4(a, b) the incident rays are traced directly to the focal plane, and the emergent wavefront has been constructed from the traced rays. In Figs. 4(c, d) the rays are traced from the entrance facet to the destination plane (see Fig. 3), at which point the emergent wavefront is constructed. This wavefront is subsequently back-propagated to the rear facet of the lens using the far field (Fraunhofer) diffraction formula. Since the incident beam in this particular example is highly aberrated, the two methods of calculation yield similar results. As a general rule, however, the incident rays should *not* be traced to the vicinity of the focal plane, where, due to significant effects of diffraction, geometric-optical methods are inadmissible.

Effect of beam tilt and wavefront curvature

Figure 5 shows cross-sectional plots of intensity, log_intensity, and phase for a $\lambda = 1.55 \mu\text{m}$ Gaussian beam arriving at the entrance pupil of the GRIN lens of Fig. 3. The incident beam's FWHM and full-aperture diameters are $D_{\text{FWHM}} = 0.639 \text{ mm}$ and $D = 2.17 \text{ mm}$, respectively. The phase plot in Fig. 5(c) contains 2λ of linear distortion (corresponding to

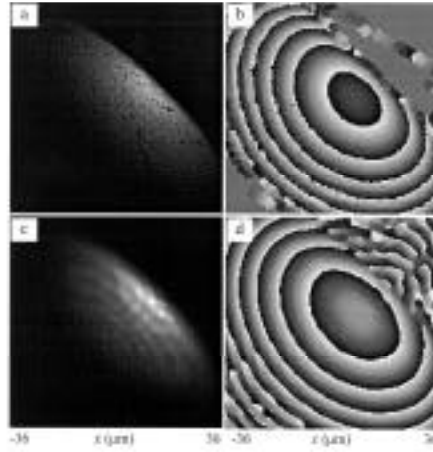


Figure 4. Using two different methods, the intensity (left) and phase (right) distributions at the focal plane of the GRIN lens of Fig.3 have been computed for the incident beam shown in Fig.2. In (a) and (b) the incident rays are traced directly to the focal plane, and the emergent wavefront is constructed from traced rays. In (c) and (d) the rays are traced from the entrance facet of the lens to the destination plane, where the emergent wavefront is constructed and subsequently back-propagated to the focal plane (i.e., rear facet) of the GRIN lens.

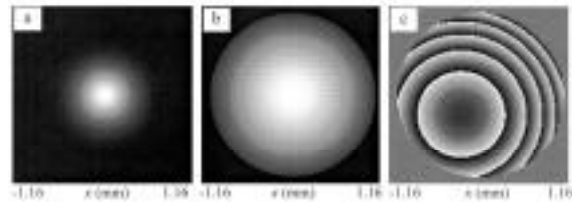


Figure 5. Plots of (a) intensity (b) log_intensity, and (c) phase of a $\lambda = 1.55 \mu\text{m}$ Gaussian beam arriving at the entrance facet of the GRIN lens. The beam has FWHM diameter $D_{\text{FWHM}} = 0.64 \text{ mm}$, full-aperture diameter $D = 2.17 \text{ mm}$, 2λ of linear distortion (i.e., 0.16° of tilt), and 3λ of Seidel curvature (i.e., $R_c = 127 \text{ mm}$).

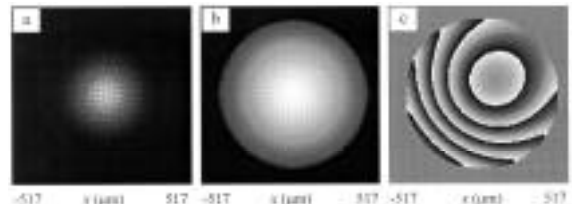


Figure 6. Plots of (a) intensity, (b) log_intensity, and (c) phase of the emergent beam at the destination plane, located 2.0 mm beyond the exit facet of the GRIN lens of Fig.3. Since the beam is highly divergent at this point, its curvature phase-factor ($R_c = 2.046 \text{ mm}$) has been subtracted from the phase plot.

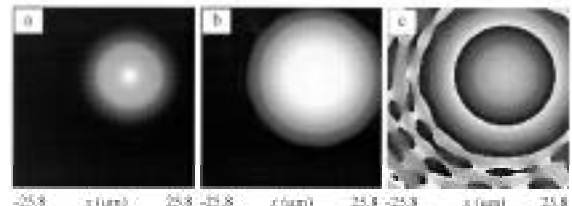


Figure 7. Plots of (a) intensity, (b) log_intensity, and (c) phase of the focused spot at the rear facet of the GRIN lens of Fig.3. To compute these distributions, the beam displayed in Fig.6 has been back-propagated a distance of 2.0 mm (i.e., from the destination plane to the rear facet of the GRIN lens).

0.16° of tilt), and 3λ of Seidel curvature (corresponding to a radius of curvature $R_c = 127 \text{ mm}$). After tracing the incident rays to the destination plane (located 2.0 mm away from the exit facet of the GRIN lens, within a homogeneous medium of refractive index $n = 1.5$) we obtain the plots of intensity, log_intensity, and phase displayed in Fig. 6. The emerging beam at the destination plane is divergent, and its curvature phase-factor ($R_c = 2.046 \text{ mm}$) has been subtracted from the phase plot in Fig. 6(c). For the full aperture of the incident beam ($D = 2.17 \text{ mm}$), the emergent beam diameter of 0.86 mm at the destination plane represents a divergence cone angle $\theta = 24.3^\circ$, yielding an effective numerical aperture $\text{NA} = n \sin(\theta/2) = 0.32$.

When the light amplitude distribution of Fig. 6 is back-propagated (from the destination plane to the rear facet of the GRIN lens), one obtains the focused spot distribution shown in Fig. 7. These cross-sectional plots show intensity, log_intensity, and phase of the focused beam at the rear facet of the GRIN lens. The $9.2 \mu\text{m}$ shift of the beam center away from the center of coordinates is a consequence of the 0.16° tilt of the incident beam. Also, the 3λ curvature of the incident beam is seen to have resulted in a substantial enlargement of the focused spot.

Effect of beam size and astigmatism

Figure 8 shows plots of intensity (left column), log_intensity (middle column), and phase (right column) at the rear facet of the GRIN lens of Fig. 3 under three different conditions. In the first row, the assumed incident Gaussian beam is fairly large ($D_{\text{FWHM}} = 1.37 \text{ mm}$, full aperture $D = 3.0 \text{ mm}$), and has no aberrations. The focused spot, however, is degraded by $\sim 105 \mu\text{m}$ of defocus, both of which are consequences of the large diameter of the incident beam. (The GRIN's parabolic index profile is not optimum for diffraction-limited focusing at large aperture, nor is the selected length of the lens appropriate for wide-aperture applications, where the best focus is found to be inside the

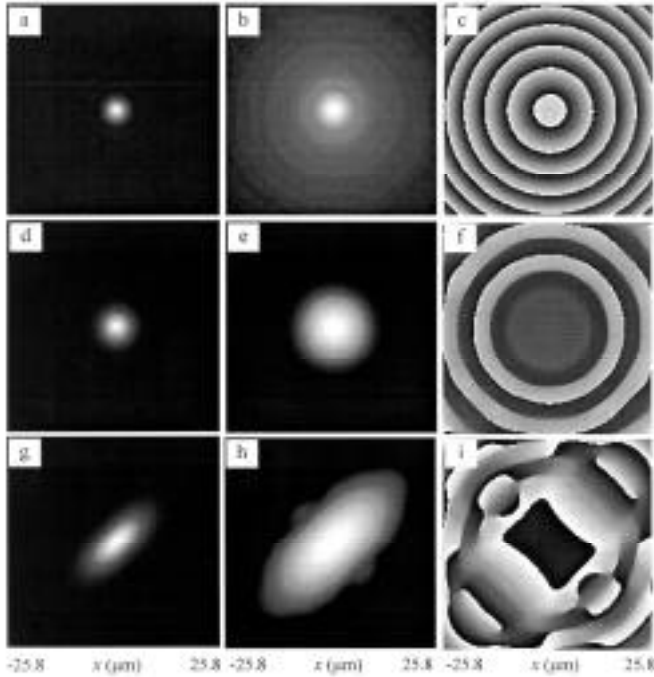


Figure 8. Plots of intensity (left),log_intensity (middle),and phase (right) at the rear facet of the GRIN lens of Fig.3.(Top row) Incident beam diameters $D_{FWHM} = 1.37$ mm, $D = 3.0$ mm,no aberrations other than the spherical aberration and $-105 \mu\text{m}$ of defocus introduced by the lens itself.(Middle row) Incident beam diameters $D_{FWHM} = 0.365$ mm, $D = 2.17$ mm, no aberrations. (Bottom row) Same as the middle row, except for the presence of 4λ of Seidel astigmatism (i.e.,cylinder) on the incident wavefront.

lens.) The large NA of the lens is responsible for the poor efficiency of coupling into the fiber obtained in this case ($\eta \sim 27\%$).

The second row of Fig. 8 shows profiles of the focused spot for a smaller incident beam, having $D_{FWHM} = 0.365$ mm, $D = 2.17$ mm, and no aberrations. This focused spot is well matched to the fiber's mode profile, yielding a large coupling efficiency ($\eta \sim 99\%$). Finally, the third row of Fig. 8 shows the focused spot profile computed for the same incident beam as above ($D_{FWHM} = 0.365$ mm, $D = 2.17$ mm), to which 4λ of Seidel astigmatism (i.e., wavefront cylinder) has been added. Astigmatism reduces the computed coupling efficiency to $\eta \sim 69\%$.

Tolerance for beam decenter, tilt, and defocus

We computed the coupling efficiency (into a single-mode fiber) of the GRIN lens of Fig. 1 for an incident Gaussian beam as function of the beam diameter D_{FWHM} . From these results the optimum beam size that yielded the largest η was identified. Subsequently, we studied tolerances of the lens (at the optimum beam size) by com-

puting η as function of the incident beam decenter, tilt, and wavefront curvature (i.e., defocus). These results indicate the sensitivity of the lens-fiber module to alignment errors.

Figure 9 shows the various performance curves of the GRIN lens of Fig. 1. Shown in Fig. 9(a) is a plot of η versus D_{FWHM} ; the optimum beam diameter is seen to be $\sim 365 \mu\text{m}$. The remaining frames in Fig. 9 are computed at this optimum beam size. Figure 9(b) shows the sensitivity of η to beam decenter. Note that a decenter of $\sim 250 \mu\text{m}$ is sufficient to reduce η by about 50%. The plot of η versus beam tilt in Fig. 9(c) shows that a 0.15° tilt can reduce η more than tenfold. Finally, Fig. 9(d) shows that a few waves of Seidel curvature (i.e., defocus) can substantially reduce the efficiency of coupling into the fiber.

Plano-aspheric lens

Another design for a lens that can launch a collimated beam into a single-mode fiber is the plano-aspheric aplanat depicted in Fig. 10. This lens is designed to bring a $\lambda = 1.55 \mu\text{m}$ beam to diffraction-limited focus

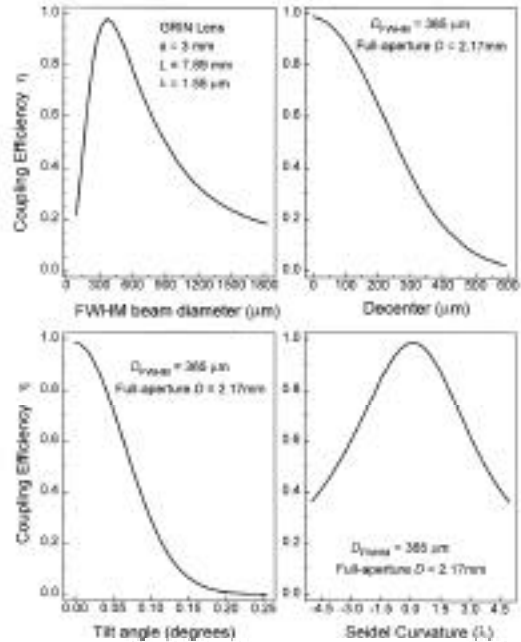


Figure 9. Characteristics of the GRIN lens of Fig.1,computed for a $\lambda = 1.55 \mu\text{m}$ incident Gaussian beam.(a) Dependence of the coupling efficiency η on the FWHM diameter of the incident beam;optimum diameter is $\sim 365 \mu\text{m}$. (b) Dependence of η on incident beam tilt decenter relative to the optic axis. (c) Variation of η with incident beam tilt. (d) Effect on η of Seidel curvature (i.e., defocus);the horizontal axis depicts the departure of the wavefront at the edge of the beam, where the assumed beam's full-aperture diameter is $D = 2.17$ mm.In (b),(c),and (d) the incident beam has $D_{FWHM} = 365 \mu\text{m}$.

at its rear facet, a plane facet to which the fiber is attached. The lens has diameter $\phi = 3.0$ mm, length $L = 5.8826$ mm, and refractive index $n = 1.673286$. The asphere parameters are: $R_c = 2.367$ mm, $K = -0.66723$, $A_4 = 2.91125 \times 10^{-3}$, $A_6 = 2.52286 \times 10^{-4}$, and $A_8 = 2.93078 \times 10^{-5}$. Figure 11(a) shows the dependence of η on incident beam diameter. Clearly, maximum efficiency is achieved at $D_{FWHM} \sim 411 \mu\text{m}$.Figure 11(b) shows the dependence of η on beam decenter, when the incident beam diameter is fixed at its optimum value of $411 \mu\text{m}$. Similarly, sensitivity to tilt at the optimum beam size is shown in Fig. 11(c), and the dependence of η on Seidel curvature is shown in Fig. 11(d). A comparison of Fig. 9 with Fig. 11 shows that the GRIN lens is nearly as good as the plano-aspheric lens, at least as far as the particular alignment tolerances studied here are concerned.

Plano-convex lens made of Gradium™ glass

Lenses made from Gradium™ glass have a refractive index gradient along their optic axis. Although this type of index gradient

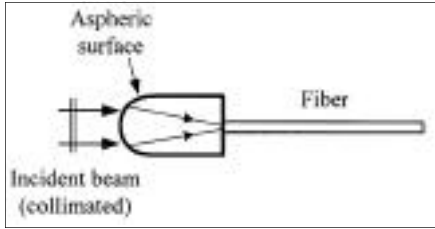


Figure 10. Plano-aspheric lens, having diameter $\phi = 3.0$ mm, length $L = 5.88$ mm, and refractive index $n = 1.673286$. The single-mode fiber is attached to the rear facet of the lens.

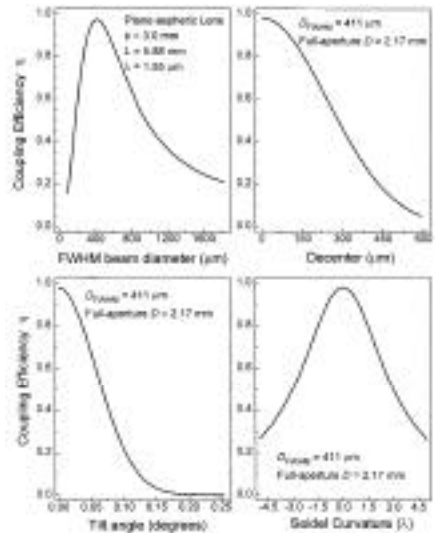


Figure 11. Characteristics of the plano-aspheric lens of Fig.10, computed for a $\lambda = 1.55 \mu\text{m}$ incident Gaussian beam. (a) Dependence of η on the FWHM diameter of the incident beam; optimum diameter is $\sim 411 \mu\text{m}$. (b) Dependence of η on incident beam decenter relative to the optic axis. (c) Variation of η with incident beam tilt. (d) Effect on η of Seidel curvature (i.e., defocus); the horizontal axis depicts the departure of the wavefront at the edge of the beam, where the assumed beam's full-aperture diameter is $D = 2.17$ mm. In (b), (c), and (d) the incident beam has $D_{\text{FWHM}} = 411 \mu\text{m}$.

does not by itself produce focusing power, it has the ability to correct aberrations and field curvature introduced by curved surfaces.

A plano-convex lens made of Gradium™ glass for focusing a collimated beam into a fiber is shown in Fig. 12. The various lens parameters are: $R_c = 3.715$ mm, $\phi = 2.6$ mm, $L = 2.9$ mm, Gradium™ glass = G14SF, $z_{\text{max}} = 5.8$ mm, and $\Delta z = 2.85$ mm. The focal point is a distance of 3.535 mm beyond the plane facet of the lens. For this lens, the dependence of η on beam size as well as its sensitivity to mis-

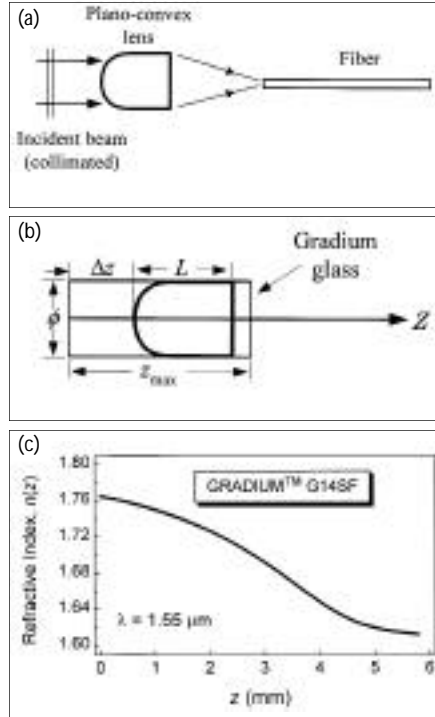


Figure 12. (a) Plano-convex lens made of Gradium™ glass is used to focus a collimated beam of light into a single-mode fiber. The front facet of the lens is spherical, having $R_c = 3.715$ mm, and the focal point is 3.535 mm beyond the rear (plane) facet of the lens. (b) The lens is fabricated by polishing into spherical shape one end of a cylindrical rod cut from a slab of Gradium glass. (c) Index profile of G14SF Gradium™ glass at $\lambda = 1.55 \mu\text{m}$. The refractive index is highest at the front vertex, decreasing nonlinearly with z as one moves toward the plane facet of the lens. When the same lens is made of homogeneous glass of refractive index $n = 1.7$, the focal point shifts by about $30 \mu\text{m}$ to the right, and the spherical aberration increases slightly.

alignments are shown in Fig. 13. The largest η is attained at $D_{\text{FWHM}} \sim 593 \mu\text{m}$. At this optimum beam size the amount of decenter that results in 50% reduction of η is $\sim 420 \mu\text{m}$, and the beam tilt that causes a 50% drop in η is $\sim 0.045^\circ$. The dependence of η on wavefront curvature may be seen in Fig. 13(d).

We also computed the various performance curves for a plano-convex lens similar to that depicted in Fig. 12, but made of homogeneous glass ($n = 1.7$) instead of the Gradium™ material. The focal point of this homogeneous plano-convex lens was found at 3.565 mm beyond its plane facet, namely, its focal length is $\sim 30 \mu\text{m}$ greater than that of the Gradium lens. Once again the optimum beam size was found at $D_{\text{FWHM}} \sim 593 \mu\text{m}$. The other

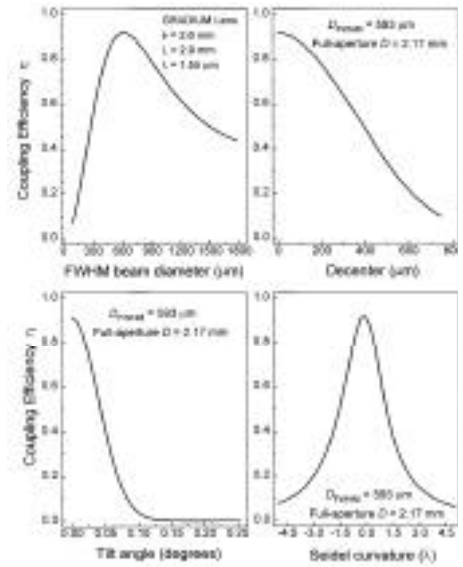


Figure 13. Characteristics of the plano-convex Gradium™ lens of Fig. 12, computed for a $\lambda = 1.55 \mu\text{m}$ incident Gaussian beam. (a) Dependence of η on the FWHM diameter of the incident beam; optimum diameter is $\sim 593 \mu\text{m}$. (b) Dependence of η on incident beam decenter relative to the optic axis. (c) Variation of η with incident beam tilt. (d) Effect on η of Seidel curvature (i.e., defocus); the horizontal axis depicts the departure of the wavefront at the edge of the beam, where the assumed beam's full-aperture diameter is $D = 2.17$ mm. In (b), (c), and (d) the incident beam has $D_{\text{FWHM}} = 593 \mu\text{m}$.

characteristics of the lens were also very similar to those of the Gradium™ lens. Apparently, the use of Gradium™ glass in this particular application does not result in any substantial improvements.

Acknowledgments

The author is grateful to Jeffrey Wilde of Capella Corp. and Jose Sasian of the Optical Sciences Center for helpful discussions. Thanks are due to Kenji Konno of the Optical Sciences Center for designing the plano-aspheric lens depicted in Fig. 10.

References

1. H. Kogelnik, in Proc. Symposium on Quasi-Optics, series **VR14**, 333-47, (1964).
2. W. L. Emkey, J. Lightwave Technology **LT-1** (2), 436-43, (1983).
3. D. T. Neilson, Applied Optics **38**, 2282-6, (1999).
4. The computer simulations reported in this article were performed with DIFFRACT™, a product of MM Research, Inc., Tucson, Arizona.

OPN contributing editor Masud Mansuripur is a professor of Optical Sciences at the University of Arizona in Tucson and president of MM Research, Inc. <masud@u.arizona.edu>.